ADVANCED ENERGY MATERIALS
www.advenergymat.de

Optimized Temperature Effect of Li-Ion Diffusion with Layer Distance in $Li(Ni_xMn_yCo_z)O_2$ Cathode Materials for High Performance Li-Ion Battery

Suihan Cui, Yi Wei, Tongchao Liu, Wenjun Deng, Zongxiang Hu, Yantao Su, Hao Li, Maofan Li, Hua Guo, Yandong Duan, Weidong Wang, Mumin Rao, Jiaxin Zheng, Xinwei Wang,* and Feng Pan**

Understanding and optimizing the temperature effects of Li-ion diffusion by analyzing crystal structures of layered $Li(Ni_xMn_yCo_z)O_2$ (NMC) ($x + y + z = 1$) materials is important to develop advanced rechargeable Li-ion batteries (LIBs) for multi-temperature applications with high power density. Combined with experiments and ab initio calculations, the layer distances and kinetics of Li-ion diffusion of $LiNi_xMn_yCo_zO_2$ (NMC) materials in different states of Li-ion de-intercalation and temperatures are investigated systematically. An improved model is also developed to reduce the system error of the "Galvanostatic Intermittent Titration Technique" with a correction of NMC particle size distribution. The Li-ion diffusion coefficients of all the NMC materials are measured from −25 to 50 °C. It is found that the Li-ion diffusion coefficient of $LiNi_{0.6}Mn_{0.2}Co_{0.2}O_2$ is the largest with the minimum temperature effect. Ab initio calculations and XRD measurements indicate that the larger Li slab space benefits to Li-ion diffusion with minimum temperature effect in layered NMC materials.

1. Introduction

Li-ion batteries (LIBs) are now widely used in portable electronic industry, plug-in hybrid vehicles (PHEVs), and electric vehicles (EVs)[1] all over the world due to their advantages such as high energy density, high voltage, and long cycle life.[2] As one of the most widely used cathode materials, $LiNi_xMn_yCo_zO_2$ (labeled as NMC) has been investigated extensively, due to their high reversible capacity, good environmental compatibility, and relatively high Li-ion diffusivity. In the previous works, different kinds of NMC materials with different content ratio of Ni, Co, and Mn have been developed, and their electrochemical properties have also been studied, such as $Li(Ni_{1/3}Mn_{1/3}Co_{1/3})O_2$ (111),[3,4] $Li(Ni_{0.4}Mn_{0.4}Co_{0.2})O_2$ (442),[5] $Li(Ni_{0.42}Mn_{0.42}Co_{0.16})O_2$ (552),[6] $Li(Ni_{0.5}Mn_{0.3}Co_{0.2})O_2$ (532),[7] $Li(Ni_{0.6}Mn_{0.2}Co_{0.2})O_2$ (622),[8] and $Li(Ni_{0.7}Mn_{0.15}Co_{0.15})O_2$ (71515).[9] For example, Noh et al. compared the electrochemical properties including the Li-ion diffusion coefficient, capacity retention, and electrochemical stabilities (25 to 55 °C) of layered NMC cathode materials ((111), (532), (622), (71515), (811) and $Li(Ni_{0.85}Mn_{0.075}Co_{0.075})O_2$) at room temperature and found that the Ni content had a great influence on the electrochemical properties.[10]

Solid phase diffusion coefficient (D_s) is one of the most important parameters for the active materials of the LIBs, as it determines the charge and discharge rate capability directly. In particular, for high power density applications, fast Li-ion transport in cathode materials is a key factor and must be needed. As a result, many experimental and theoretical works have been devoted to investigating the Li-ion diffusion properties in layered cathode materials.[11,12] However, to the best of our knowledge, there is little work reported to study the relationship between the layer distance and kinetics of Li-ion diffusion in different temperatures of layered NMC cathode materials systematically, which is important for LIBs applied in multi-temperature environments.

At the same time, in order to measure D_s accurately, many methods such as galvanostatic intermittent titration technique (GITT),[3,13–16] potentiostatic intermittent titration technique (PITT),[14,17] electrochemical impedance spectroscopy,[18] and cyclic voltammetry[19] have been developed in the past decades. Although factors such as the inaccuracy of the assumptions,

S. Cui, Y. Wei, T. Liu, W. Deng, Z. Hu, Y. Su, H. Li, M. Li, H. Guo, Dr. Y. Duan, Prof. J. Zheng, Prof. X. Wang, Prof. F. Pan
School of Advanced Materials
Peking University
Shenzhen Graduate School
Shenzhen 518055, P. R. China
E-mail: zhengjx@pkusz.edu.cn; wangxw@pkusz.edu.cn; panfeng@pkusz.edu.cn
Dr. W. Wang
Shenzhen Tianjiao Technology Development Co., Ltd.
Shenzhen 518119, P. R. China
Dr. M. Rao
Shenzhen OptimumNano Energy Co., Ltd.
Shenzhen 518118, P. R. China

DOI: 10.1002/aenm.201501309

the distribution of the NMC particle size, the jitter of the cell voltage, and so on, may cause the measurement errors, however, no better methods can replace these methods mentioned above. Despite the existence of the errors and the disadvantage of long-time waiting, the results measured by GITT are still well accepted by scientists up to now. Besides, it is easier to implement compared with the other methods. Meanwhile, as different previous researches used different experiment conditions, different methods and different instruments, the GITT results always had a few orders of magnitude differences, and it is also difficult to compare the diffusion properties of different NMC materials from previous reported works. Therefore, it is hard to distinguish that which material has the best Li-ion diffusivity.

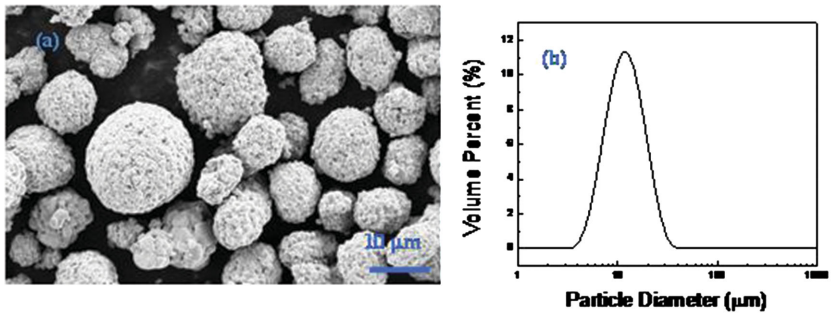

Figure 1. a) SEM of 622, b) the particle size distribution of $Li(Ni_{0.6}Mn_{0.2}Co_{0.2})O_2$.

Here, we combined with experiments and ab initio calculations to investigate the Li-ion diffusion of NMC materials in different temperatures at the different states of Li-ion de-intercalation systematically for the first time. The D_s values of a series of different NMC materials (111, 442, 552, 532, 622, and 71515) at different temperatures from –25 °C (248 K) to 50 °C (323 K) are measured by using the improved GITT method, which is developed to employ an improved model to reduce the system error of GITT method with a correction of NMC particle size distribution. After comparing the kinetics properties of different NMC materials, it is found that 622 shows the highest Li-ion diffusivity with the minimum temperature dependence. Furthermore, both ab initio calculations and X-ray diffraction (XRD) measurements suggest that the Li slab space of the NMC layered material plays a great role on the Li-ion diffusion property versus temperature.

2. Results and Discussion

Figure 1a shows the Scanning electron microscope (SEM) of 622. As the form of different NMC materials is very similar, we take 622 as an example. The spherical particles are the secondary particles which consist of a lot of primary particles with a small grain for each of them. Besides, the SEM indicates that the secondary particles size is heterogeneous and most secondary particles have a diameter about 5–20 μm, as shown in Figure 1b.

Figure 2a–c shows the Li-ion diffusion coefficient (D_s) versus different state of Li-ion de-intercalation (δ) of $Li_{1-\delta}(Ni_xMn_yCo_z)O_2$ ($0 \le \delta \le 1$) at 50, 25, and 0 °C, respectively. The Li-ion diffusion coefficients of all the NMC materials are in the range of about 1–10 × 10^{-11} cm^2 s^{-1}. The diffusion coefficient of 622 is the largest among all the NMC materials we tested no matter at which temperature, while 111 is the smallest at 25 and 0 °C. The Li-ion diffusion coefficient increases with the temperature (Figure 2d). At the high temperature of 50 °C, the diffusion coefficient becomes greater than that at 25 °C. Meanwhile, the diffusion coefficient at low temperatures (0 and –25 °C) is less than that at 25 °C (Figure 2b). According to the equation between the diffusion coefficient and the temperature (see Equation (8) in Experimental Section), lower temperature means smaller diffusion coefficient. With the rise of the temperature, Li-ions can diffuse more easily.

For the same material, the δ dependence increases as the temperature decreases. At 50 °C, the δ dependence of the Li-ion diffusion coefficient of all the NMC materials is very small, while the Li-ion diffusion coefficient changes a lot with δ at 0 °C. That is because δ is not the only factor that affects the Li-ion diffusion coefficient. When the Li-ion diffusion coefficient is large enough, the temperature dominates the mechanism instead of δ. Meanwhile, the Li-ion diffusion coefficient increases with the increase of δ. Interestingly, we found that the temperature fluctuation and the δ dependence of 622 diffusion coefficient were the smallest at 25 °C, while the variations of the other NMC materials are much larger. This implied that 622 has the largest applied range for different temperatures.

To further study 622 temperature effect of Li-ion diffusion coefficient, D_s versus temperatures from –25 to 50 °C is shown in Figure 2d, indicating that the increase of the Li-ion diffusion coefficient is less than an order of magnitude. The diffusion coefficient of 622 still has 2 × 10^{-11} cm^2 s^{-1} at –25 °C. Therefore, in a certain temperature range (such as –25 to 50 °C), 622 can keep a relatively larger Li-ion diffusion coefficient. Hence, from the perspective of the experiment results, intuitively, 622 is the most promising NMC material for multi-temperature applications with higher Li-ion diffusivity and lower temperature effect. The rate capabilities of all the NMC materials were also tested, as shown in Figure 2e,f. We can see that the rate capability of 622 is the best, with the least capacity loss among all the NMC materials from 1 to 5 C, as it is shown in Figure 2e. Though the capacity of 71515 (147 mAh g^{-1}) is larger than that of 622 (142 mAh g^{-1}) at 1 C, the capacity of 622 (107 mAh g^{-1}) becomes larger than that of 71515 (105 mAh g^{-1}) at 5 C. Figure 2f shows the rate capability of 622 and 71515 at 0 °C, and note that the capacity of 622 (55 mAh g^{-1}) is much bigger than that of 71515 (19 mAh g^{-1}) at 5 C.

Among all NMCs, 532 is one of most widely used cathode materials in LIB applications. Here, we compare the Li-ion diffusion coefficients and related temperature effect of 622 and 532 in the following study. According to Equation (8) in the Experimental Section, if we take logarithm on both sides of the equation at the same time, we can plot the logarithm of the Li-ion diffusion coefficient versus the reciprocal of the temperature, in which the slope of the new straight line corresponds to the absolute value of E_a, as shown in Equation (1).

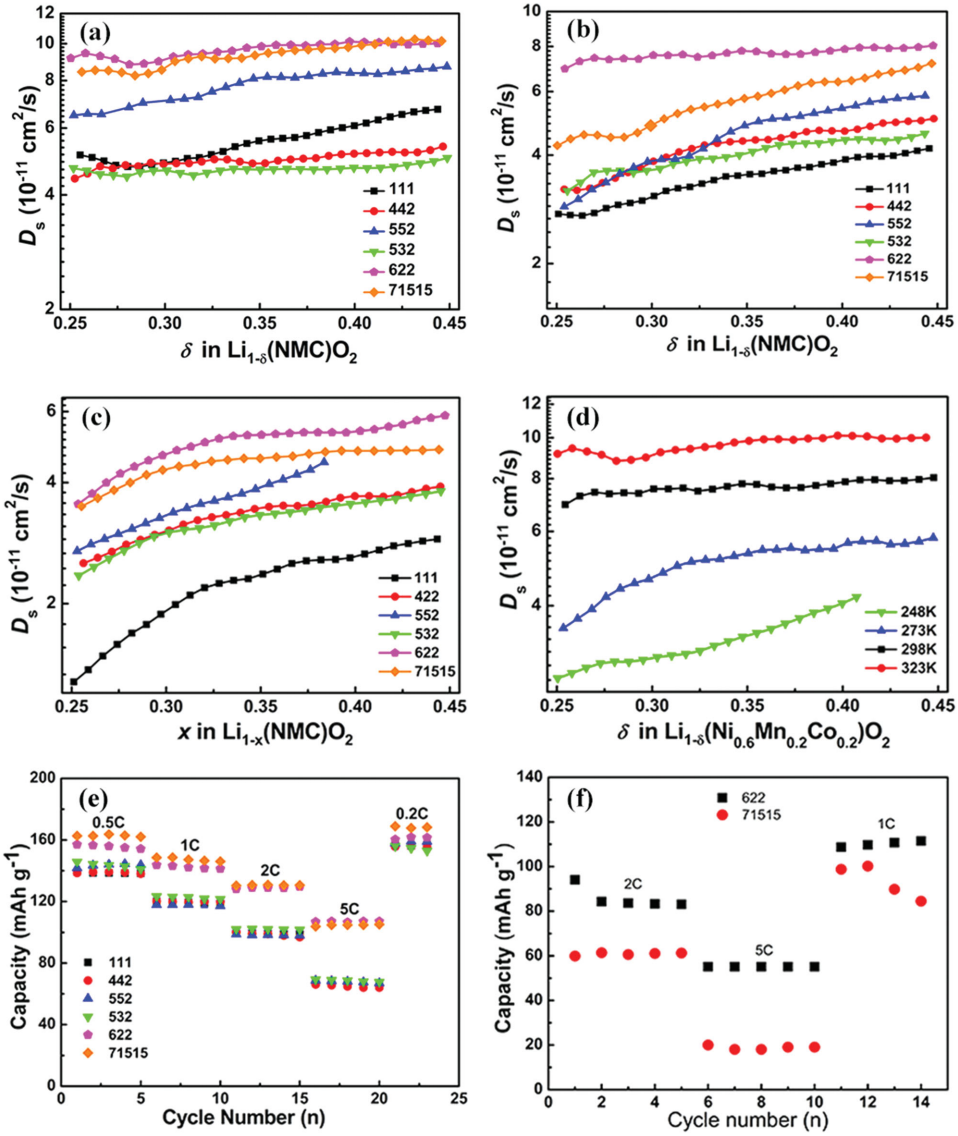

Figure 2. Diffusion coefficient of different materials versus state of charge in a) 50 °C (323 K), b) 25 °C (298 K), c) 0 °C (273 K), and d) shows D_s of 622 in different temperature. Rate capability of e) all NMC materials at 25 °C and f) 622 and 71515 at 0 °C.

$$\log(D_s) = \log(D_0) - \frac{E_a}{K}\frac{1}{T} \quad (1)$$

E_a (eV) is the activation energy for diffusion, k (eV K^{-1}) is the Boltzmann constant, and D_0 is the diffusion coefficient when the temperature goes to infinite.

The calculation and GITT results of 532 and 622 at $\delta = 0.33$ are shown in **Figure 3**a,b, respectively, in which all curves show almost linear and the slope of 532 is slightly larger than that of 622, suggesting that the value of E_a of 532 is larger so as to be easier to be affected by the temperature. Note that the Li-ion diffusion coefficient of calculation is 1–2 orders of magnitude larger than that of GITT, which is mainly attributed to the systematic error which exists between the experiment and the calculation (see Section 4.1). Although the value of the slope from calculation is much bigger than that of measurement, the variation trends of the Li-ion diffusion coefficients of 532 and 622 by measurement and calculation are same.

The question is why the Li-ion diffusion coefficient of 622 is larger than that of 532 and other NMCs to be the largest with the minimum temperature effect in all the NMC materials. The mechanism is investigated according to relationship of layer distance structure versus Li-ion diffusion property by combination with the experimental measurements and ab initio calculations as below.

As shown in Equation (1), the Li-ion diffusion coefficient is related to the effective activation energy E_a. As indicated in our previous work,[12] there are two kinds of Li-ion diffusion pathways in such layered structures, namely, Li-ion diffuses from one octahedral site to next site through the oxygen dumbbell or an intermediate tetrahedral site, in which Li-ions tend to choose oxygen dumbbell hopping at the early stage of

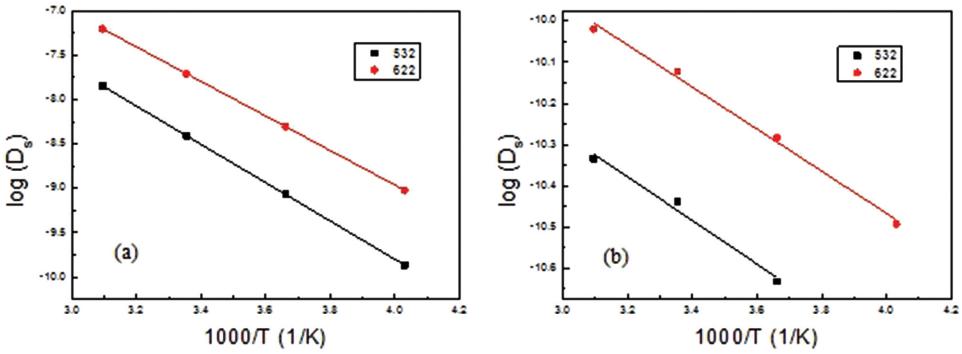

Figure 3. Diffusion coefficient comparison of 532 and 622 at $\delta = 0.33$ in a) ab initio calculation, b) GITT test.

charging (delithiation), and tetrahedral site hopping (TSH) begins to dominate when more than 1/3 Li-ions ($\delta > 0.33$) are extracted (**Figure 4**). The size of the oxygen dumbbell or the tetrahedral site (strain effect) as well as the electrostatic interaction between Li-ion in the activated state and the transition metal cation would contribute to the activation energy. As a result, the activation energy of Li-ions along this pathway is closely associated with the size of Li–O tetrahedrons and octahedrons. The oxygen atoms from upper and under layer would affect the diffusion barrier of Li. Li-ions that diffuse in narrow pathway are under larger forces, which leads to higher activation energy. In Figure 4b (TSH route), Li-ion diffuses from position 1 to position 3. When Li-ion is in position 2, the distance of Li and O atoms affects the work that the system has to do to transfer the Li-ion across this O atoms tetrahedron. Smaller Li slab space would decrease the size of the O atoms tetrahedron, while the energy barrier of this diffusion pathway would increase. The distance between these two O atoms is closely associated with the activation energy of this pathway. As a result, the activation barrier for Li-ion diffusion depends on the Li slab space (a type of the strain effect) and the kind of transition metals and their valence states. Previous studies[12] and Kang[20] reported that more Ni content with low valence state and large Li slab space are beneficial for Li-ion diffusion. Especially, the activation barrier is sensitive to the Li slab space. When Li slab space increases by 0.1 Å, activation energy along this pathway rises by 100 meV.[20] Here, the Ni^{3+} content is the same for 532 and 622 at $\delta = 0.33$ and 0.5. Therefore, the difference of Li-ion diffusion coefficients between the two kinds of materials must come from the difference of Li slab spaces.

As shown in Figure 4a, Li slabs and transition metal oxide slabs are distributed alternatively, in which d_1 is the thickness of transition metal oxide slab, and d_2 is the Li slab space, d_{001} is the distance of (001) plane. The relationship between d_1 and d_2 is given as

$$d_1 + d_2 = d_{001} \quad (2)$$

The XRD patterns of the six NMC materials we tested are shown in **Figure 5**a. The materials have a highly crystalline layered structure, with diffraction peaks corresponding to the R-3m space group. The splitting of the (108), (110) and (006), (102) peaks indicated well-ordered α-$NaFeO_2$ structure. The (003) peaks of different NMCs are almost at the same 2θ. Based the (003) peaks of XRD, we can find that the distances of (001) plane (d_{001}, the layer distance of NMC shown in Figure 4a) of all the NMCs are almost same around 4.74 (±0.01) Å at $\delta = 0$ as shown in **Table 1**, in which chemical lithium de-intercalation is used to control δ. Figure 5b,c shows the XRD of 532 and 622 at different δ, respectively. As δ increases, the (003) peak shifts as shown in the inset graphs. A summary of distances of (001) planes of all the NMCs with different δ by XRD is shown in

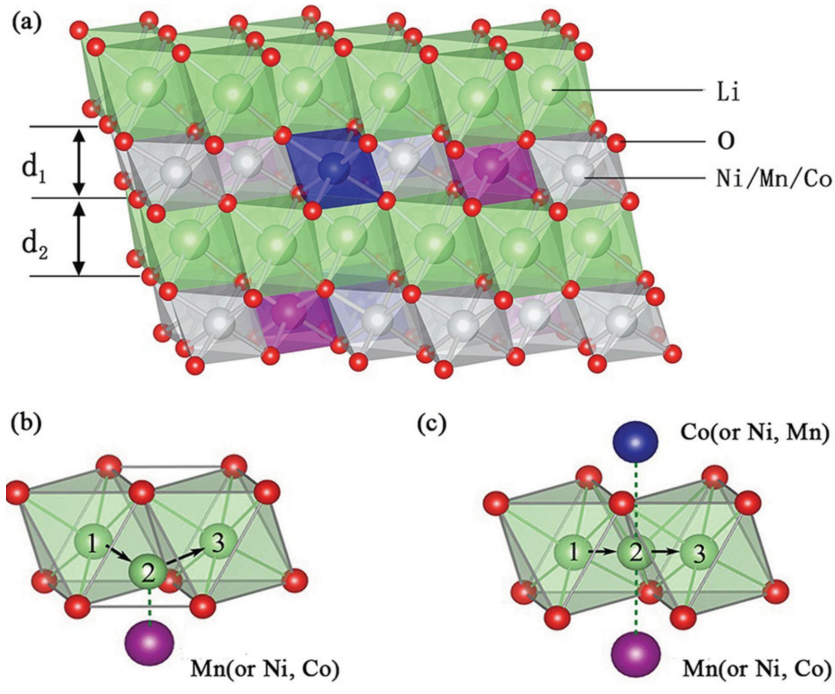

Figure 4. a) Lattice of NMC layered structure. Green atoms, Li; red atoms, O; silver/purple/blue atoms, Ni/Mn/Co transition metals. b) Tetrahedral site pathway and c) oxygen dumbbell pathway for Li-ion diffusion in NMC layered structure.

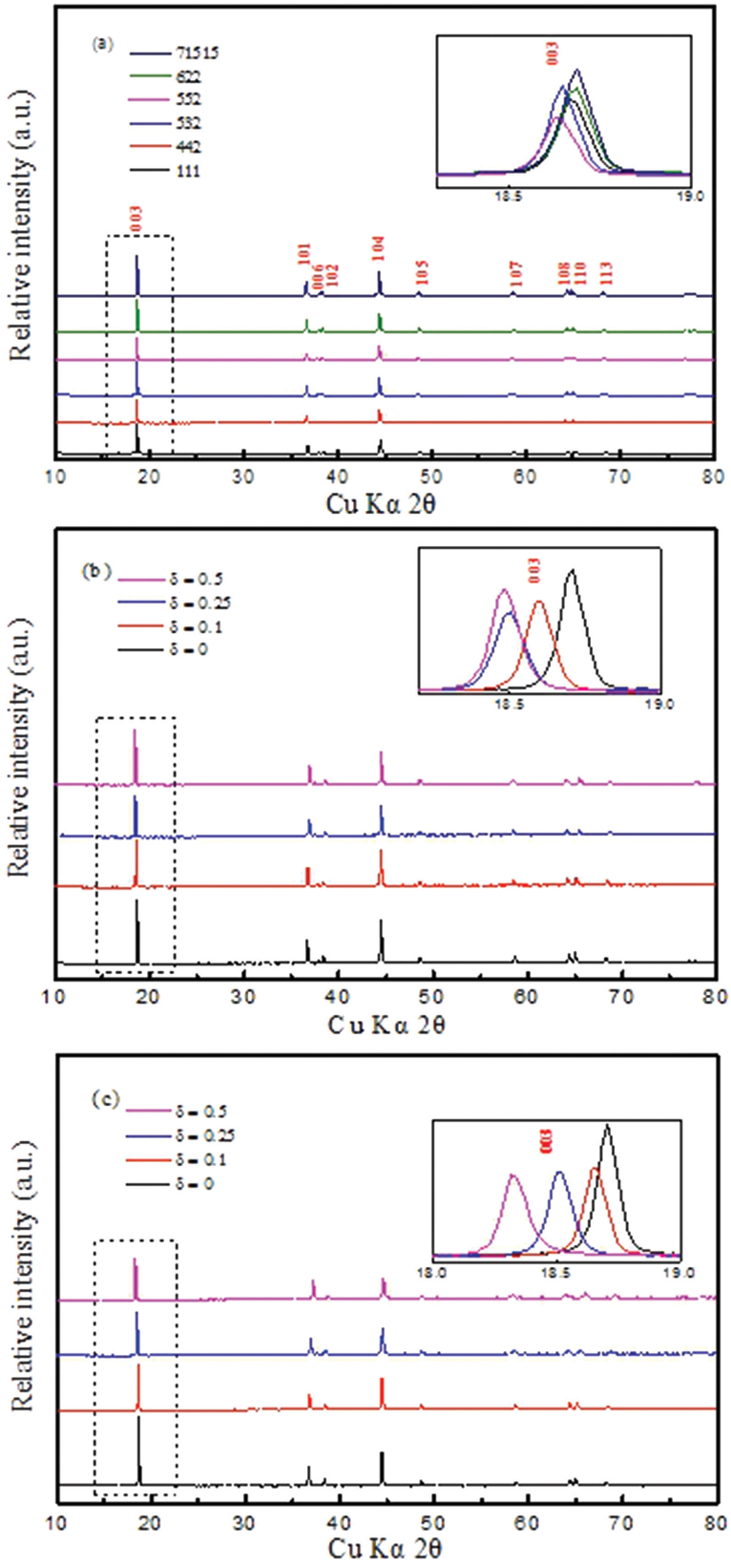

Figure 5. a) XRD of NMC materials. XRD of b) 532 and c) 622 after chemical lithium de-intercalation. The data in the dashed line box is magnified in the inset graph.

Table 1, in which displacements of the (001) peaks shift to lower diffraction angles, meaning that the (001) plane distances of all the NMCs increase with Li-ion de-intercalation process (increasing δ). Note that the (001) plane distances of 622 increase more than that of 532 with the increasing δ.

By using ab initio calculation models, the (001) plane distances and Li slab spaces of different NMCs are calculated as shown in **Tables 2** and **3**, respectively. Note that measured (001) plane distances of 333, 442, and 552 around 4.74 (±0.01) Å are a little bit larger than those of calculation around 4.68 (±0.02) Å, in which x(Ni) = y(Mn) in $Li(Ni_xMn_yCo_z)O_2$. However, measured and calculated (001) plane distances of NMC 532, 622, 71515 are very close around 4.73–4.78 Å at $\delta = 0$ (see Tables 1 and 2), in which x(Ni) > y(Mn) in $Li(Ni_xMn_yCo_z)O_2$. The difference of transition metal oxide slab is caused by ionic radius of Ni, Co, and Mn. According to Equation (2), when transition metal oxide slab is smaller, Li slab would share larger space. The calculation data of transition metal oxide slabs at δ = 0, 0.33, and 0.5 is shown in Table 3. (110) plane distance measured by XRD at δ = 0, 0.1, 0.25, and 0.5 can indirectly indicate distances of transition metal oxidation octahedral inside their slabs as shown in Table S4 (Supporting Information).

In our experiments, we found that with the increase of δ, d_{001} of all NMCs become bigger (see Table 1), and the calculations also show that d_{001} increases with δ (Table 2). However, transition metal oxide slabs (d_1) of NMCs decrease with the increase of δ because the Ni ionic radius decreases during the Ni oxidation from Ni^{2+} to Ni^{3+}, or Ni^{3+} to Ni^{4+}. d_1 and d_2 of NMC materials are calculated, as shown in Table 3, in which the transition slab space (d_1) decreases as the increasing of δ. According to Equation (2), Li slab space increases with the increasing of δ, which is consistence with the variation of d_2 in Table 3. Note that d_1 of 111 is the smallest. That is because in NMC111, the content of Mn^{4+} and Co^{3+} is the largest among all the NMC materials. Due to the smaller size of Mn^{4+} (53 pm) and Co^{3+} (54.5 pm) compared with Ni^{3+} (60 pm) and Ni^{2+} (69 pm), NMC111 has the smallest transition slab space (d_1). These calculation and measurement data indicate that transition metal oxide slab (d_1) of 622 is the smallest among all the NMC materials except 111, while the Li slab (d_2) of 622 is largest comparing to that of 532 and 71515 (see Table 3).

The question is why the layer distance (d_{001}) and the Li slab (d_2) of 622 at various Li-ion de-intercalation(δ) are larger than that of other NMCs. As Ni content rises in NMC material

Table 1. The distance of (001) plane of a series of NMC materials analyzed from XRD. The value of the error is 0.01 Å.

δ	(001) plane distance [Å]					
	333	442	552	532	622	71515
0	4.729	4.751	4.745	4.753	4.735	4.734
0.1	4.773	4.777	4.783	4.769	4.754	4.757
0.25	4.798	4.790	4.797	4.795	4.791	4.777
0.5	4.819	4.810	4.812	4.799	4.839	4.828

Table 2. The (001) plane distance in different NMC with $\delta = 0$, 0.33, and 0.5 from ab initio calculations.

δ	(001) plane distance [Å]					
	333	442	552	532	622	71515
0	4.664	4.705	4.686	4.766	4.785	4.768
0.33	4.672	4.721	4.708	4.778	4.792	4.781
0.5	4.678	4.729	4.717	4.788	4.797	4.787

Table 3. Transition slab space (d_1) and Li slab space (d_2) in ab initio calculation with $\delta = 0$, 0.33, and 0.5.

	333	442	552	532	622	71515	
d_1 [Å] (Calculated)	$\delta = 0$	2.040	2.091	2.076	2.154	2.084	2.215
	$\delta = 0.33$	2.032	2.080	2.046	2.099	2.076	2.120
	$\delta = 0.5$	2.028	2.073	2.033	2.069	2.065	2.096
d_2 [Å] (Calculated)	$\delta = 0$	2.624	2.614	2.610	2.612	2.701	2.553
	$\delta = 0.33$	2.640	2.641	2.662	2.679	2.716	2.661
	$\delta = 0.5$	2.650	2.656	2.684	2.719	2.732	2.691

Table 4. The average activation energy of Li-ions in different NMC.

	Average activation energy [meV]				
	111	442	532	622	71515
$\delta = 0.33$	514	495	503	475	484
$\delta = 0.5$			471	457	

from 532–622–71515–811, average transition ions radius increase because ionic radius of Ni^{2+} and Ni^{3+} is higher than those of Co^{3+} and Mn^{4+} as shown in Table S1 (Supporting Information). However, as the valence of Ni rises, it causes the average radius of Ni to decrease. These two mechanisms compete with each other, and there is a balance point near 622 which results in that Li slab space in 622 is larger than those in 532 and 71515.

The height of Li–O octahedrons is used to indicate the Li slab space. So the size of Li–O octahedrons and tetrahedrons along the Li-ions diffusion pathway is closely associated with the activation energy of Li-ions. For example, if the size of Li–O octahedrons reduces, the interaction between Li atoms and O atoms would increase. Therefore, Li-ions in 622 can diffuse easily due to the larger size of Li–O octahedrons and tetrahedrons than other NMC materials. On the other hand, Li slab space changes with the δ variation. Li-ions diffusion is accompanied by electrons transfer and redox of transition metal ions, and Li slab gets larger in the early stage of charging process due to the removal of O^{2-}–Li^{+}–O^{2-} bonds across the slab, which is consistent with the variation of d_2 in Table 3. The activation energies of Li-ions diffusion of 532, 622 are calculated when $\delta = 0.33$ and 0.5 along TSH pathway with Ni atom nearby as shown in **Table 4**, along which diffusion pathways with Ni atom are the advantageous pathways with low activation energy in NMC materials.[12] Obviously, the activation energy of 622 is much lower than that of 532 due to the larger layer distances.

Temperature effects of D_s in NMC materials are shown in Figure 2, in which the variation of D_s at 0 °C is larger than those at 50 °C indicating that the Li-ion diffusion is more likely to rely on the Li slab space at low temperature, because the thermal motion of Li-ions is one of the factors that facilitate the diffusion process. Ions at high temperature can diffuse spontaneously even self-destruct. It can be concluded that D_s is dominated by the increase of δ at low temperature such as 0 °C. When the temperature rise exceeds a threshold value, D_s becomes not so sensitive to δ and the variation of D_s is smaller when δ increases. Interestingly, the curve of D_s versus δ variation is flatter for 622 compared to other NMC materials (Figure 2b) at each temperature. The spacing between Li slabs is one of the important factors that affects the activation energy.[12,20] If the spacing is enlarged, the energy barrier will be lowered, so Li-ions can migrate more easily to lead to less sensitive to the Li slab space variation during the de-intercalation process. Therefore, 622 is the most promising NMC materials, for it has a larger Li-ion diffusion coefficient, the minimum temperature dependence, a better thermal adaptability and a smaller δ dependence.

3. Conclusion

Li-ion diffusion properties versus layer distance for a series of NMC materials at different temperatures are studied systematically for the first time. Among all the NMC materials, the Li-ion diffusion coefficient of NMC622 is the largest with a smaller fluctuation with the temperature. Our experimental measurements

and ab initio calculations suggest that the large Li slab space accounts for the large Li-ion diffusivity with lower the activation energy along the diffusion pathway. This study reveals that a large Li slab space would facilitate the Li-ion diffusion with less temperature dependence and also predicts that 622 is the most promising materials for LIBs applied in multi-temperature environments.

4. Experimental Section

The series of NMC were synthesized by the co-precipitation method followed by solid-state reaction.[21] The 3%–5% excess of lithium was added in order to make the molar ratio for Li / (Ni + Mn + Co) around unity. The sintering procedure was done at 800 °C for 8–12 h and then the sample was quickly cooled down to the room temperature. The synthesis conditions for these NMC cathode materials (111, 442, 552, 532, 622, and 71515) were the same, so the influence of the synthesis temperature to the *d*-space and diffusion properties is little. Electrochemical experiments were performed using cells consisting of cathode electrode made of NMC, anode electrode of metal Li and electrolyte of EC: DEC.

Electrochemical measurements were carried out by MACCOR battery test cabinet (Model MC-16 Battery Test System, 5 V, 5 A). The electrochemical cells are consisted of NMC and Li metal as the positive electrode and negative electrode, respectively. The electrolyte was $LiPF_6$ in EC: DEC mixture solvent. During the GITT experiments, the cells were kept in a thermotank (RKS-80L, 220 V, 50 Hz) to guarantee that the temperature was constant during the measurements. Prior to the measurements, all the cells were activated by 3 charge/discharge cycles, and then they were charged again to 4.35 V for the GITT measurements. During the GITT measurements, the cells were repeatedly discharged for 15 min at 0.05 C and rested for 45 min, until the voltage reached 3.3 V. SEM (ZEISS SUPRA 55) and laser particle analyzer (Mastersizer3000E) were used to determine the homogeneity and distribution of the particle diameters. X-ray diffraction (D8 Advance) was used to measure the spacing between layer distances of the NMC materials at different state of Li-ion deintercalation of $Li_{1-\delta}(Ni_xMn_yCo_z)O_2$ ($0 \le \delta \le 1$). Element analysis by Inductive Coupled Plasma Emission Spectrometer atomic emission spectrometer (ICP-aes: JY2000–2) was used to measure the amount of Li after the chemical lithium deintercalation which was handled by stirring the NMC powders in a series of different concentration acetonitrile solution of NO_2BF_4 for 24 h.

Accuracy Improvement of GITT: As the cell is discharged at a constant current, the voltage is a function of time. Assuming that the diffusion in each solid NMC particle is a 1D diffusion process,[16] and neglecting the double-layer charging process, the charge-transfer process, and the phase transformation,[15] the D_s can be calculated by Fick's law through Equation (3).[13,14]

$$D_s = \frac{4}{\pi}\left(\frac{IV_m}{z_A F S}\right)^2 \left[\frac{(dE/d\delta)}{(dE/d\sqrt{t})}\right]^2 \quad \left(t \ll \frac{L^2}{D_s}\right) \tag{3}$$

where F (96485 C mol^{-1}) is the Faraday constant, S (cm^2) is the interfacial area between the electrode and the electrolyte of the cell, I (A) is the applied current in the GITT experiment, L (cm) is the diffusion distance, z_A is the charge number ($z_A = 1$ for Li-ions), and V_M (cm^3 mol^{-1}) is the molar volume of the NMC materials, respectively. The values of $dE/d\delta$ and $dE/d\sqrt{t}$ can be extracted from the relationships of E versus δ and E versus t, respectively. For simplicity, we also approximated that the NMC particles were all spherically shaped with particle size distribution to get the average radius of R_s.[16] This approximation was fairly reasonable, as the SEM image shown in Figure 1a. We ignored the porosity of the NMC materials. As the secondary particle is composed of primary particles which are closely packed (Figure 1a), the porosity is small. So we treat the secondary particle as a solid sphere.

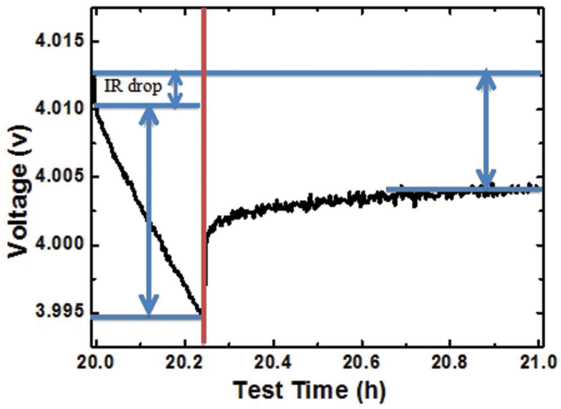

Figure 6. The voltage response of a discharge pulse in the GITT experiment. The red line divides the figure into two parts. The left part stands for the discharge pulse, while the right part stands for the rest step.

As we used fairly low current rate (0.05 C) for GITT,[14] Equation (3) can be simplified as

$$D_s = \frac{4}{\pi}\left(\frac{R_s}{3}\right)^2 \left(\frac{\Delta V_s}{\Delta V_t}\right)^2 \quad \left(\tau \ll \frac{R_s^2}{D_s}\right) \tag{4}$$

where τ (s) is the duration time for each discharge step, and the values of ΔV_s and ΔV_t can be extracted from **Figure 6**, respectively. According to Equation (4), D_s is proportional to the square of R_s. It is important to find a reasonable value of R_s to reduce the errors caused by the particle distribution. As for the particle equivalent radius (R_s), the current I in Equation (3) should be proportional to the total mass of the active particles, and therefore should be proportional to the total volume, assuming that the density is constant. While the interfacial area S in Equation (3) equals to the sum of the active particles surface area. Thus, the particle equivalent radius, R_s, should follow

$$R_s = 3\overline{V} / \overline{S} = \overline{R^3} / \overline{R^2} \tag{5}$$

where $\overline{V}$ and $\overline{S}$ are the average volume and the average surface area of the particles, respectively, and R is the radius of each NMC particle. Figure 1b shows the particle size distribution of 622 measured by the laser particle analyzer. The relationship between the volume percent and the logarithm of the particle diameter ($2R$) basically obeys Gaussian distribution. Over 99% of the 622 particles diameter is between 4.5 and 31.1 μm. Take the cubic and square of R, and calculate their average value $\overline{R^3}$ and $\overline{R^2}$ respectively according to the distribution. Therefore, R_s of 622 equals to 8.2 μm (or the equivalent diameter is 16.4 μm), based on Equation (5). Besides, Figures S6 and S7 (Supporting Information) show the SEM pictures and the particle size distribution of all the NMC samples that we test, respectively. The particle size is heterogeneous, but the distribution approximates to the Gaussian distribution. For $Li_{1-\delta}(Ni_xMn_yCo_z)O_2$, GITT is accurate to extract D_s if $0.2 < \delta < 0.5$, out of which the assumption of GITT is no longer valid,[16] as the discharge pulse can no longer be treated as a delta function, resulting large measurement errors.

Due to the factors such as the inaccuracy of the assumptions, the distribution of the NMC particle size, the jitter of the cell voltage, and so on, the GITT measurement still has its model errors. For example, the size of the NMC particles is heterogeneous, so it has a distribution. According to Equation (4), the error in spherical particle radius R_s affects D_s. Usually, R_s is smaller than actual radius. Besides, at the beginning and ending of the discharge, the voltage is unbalanced after 30 min rest. Despite these errors, no better method than GITT has been developed. As a result, previous studies reported that diffusion coefficient for NMC materials is usually in the range of 10^{-8} and 10^{-11} cm^2 s^{-1} in GITT and PITT test.[10,22]

Ab Initio Calculation Details: As the accuracy of the GITT model has its limitation, the accurate data provided by GITT is a finite region ($0.2 < \delta < 0.5$).[16] Therefore, first-principle calculation is needed to serve as a necessary supplement. All ab initio calculations were performed using the Vienna ab initio simulation package (VASP).[23] Energies used for Li mobility study are calculated with the spin-polarized generalize gradient approximation to density functional theory, using the Perdew–Burke–Ernzerhof (PBE) exchange-correlation parameterization.[24] Compared with PBE, the newer WC can give improvements for lattice constants, crystal structures, and metal surface energies for solids.[25] For cohesive energies, WC is nearly as accurate as PBE. As PBE can well deal with layered $Li(Ni_xMn_yCo_z)O_2$ cathode materials (such as crystal structure, cohesive energy, and electronic structures),[26,27] we also adopt it in this work. Another reason is that WC is not implemented in VASP package, which is the most widely used ab initio package in studies of lithium batteries. Not only the PW91 and PBE functional usually can give reasonable results for battery materials, but also many well established methods are also implemented in VASP package. For example, ab initio MD and climbing-image nudged elastic band (cNEB) method[28] are two useful tools to investigate the Li-ion diffusion properties.

PBE + *U* approach is performed to calculate accurate structural properties and electronic properties with spin polarization. The *U* value of Ni, Mn, and Co is set to be 6.4, 3.5, and 3.3 eV, respectively. *U* values are applied based on the simulation parameters of $Li(Ni_xMn_yCo_z)O_2$ models from the Materials Project website (www.materialsproject.org). All the layered structure in this work are fully relaxed and optimized to reach their minimum energy with space group R3m. The plane wave cutoff energy is 450 eV. Based on the reciprocal lattice size of NMC models, *k*-points is set from $4 \times 4 \times 2$ to $6 \times 6 \times 2$, which is used for sampling in Brillouin zone. Structures with different arrangement of transition metal atoms in each layer have been tested to find those structures with the lowest total energy in every NMC materials, which make sure that all models in our calculation are the most energetically favorable structure of NMC materials. According to previous report,[26] we apply antiferromagnetic structure in our NMC layered structure to relax the lattice and calculate structural properties instead of other magnetic structures. Various experiments and calculations show that the transition metal compounds exhibit some kinds of ordering,[6,29,30] such as ower or honeycomb ordering in $LiMn_{1/2}Ni_{1/2}O_2$.[29] Taking 622 as an example, we calculated two random distribution structures. The calculated lattice parameters of them (a, b, and c) are 5.730, 12.436, and 14.021 Å and 5.740, 12.385, and 14.017 Å, respectively. The energy of the former is −659.094 eV, and the later is −659.424 eV. Comparing the lattice parameters to the ordered structure whose lattice constants, a, b, and c, are 5.781, 12.382, and 14.100 Å, respectively, we can find the difference is not significant. But the ordered structure has an obviously lower energy, −661.157 eV. Thus, in our calculations, different ordering of transition metal ions in $LiMn_xNi_yCo_zO_2$ have been tried to determine the ions arrangement in the slab. As all the ions in NMC layered structure are fully relaxed to the minimum energy, the lattice in our models is the most stable and energetically favorable structure. Structural properties can be read from these structures, such as Li slab space and transition metal slab space.

The Li-ion diffusion coefficients for these materials mentioned above were calculated by the ab initio MD simulation, which was implemented in VASP. MSD (Mean square displacement) analysis could be used to find the MSD versus time through the data from MD simulation. Time step was set to be 3 fs in MD analysis

$$\mathrm{MSD}_i = |r_i - r_0|^2 = \left(x_i^2 + y_i^2 + z_i^2\right) - \left(x_0^2 + y_0^2 + z_0^2\right) \tag{6}$$

$$D = \lim_{t\to\infty} \frac{1}{2dt} |r_i - r_0|^2 \tag{7}$$

where x_i, y_i, z_i refer to the current position of atoms and x_0, y_0, z_0 stand for the original site of atoms, $\frac{1}{2d}$ is the constant related to diffusion dimension and $d = 2$ in layered materials for 2D diffusion.

As a result of diffusion between Li-ions position, the diffusion coefficient depends on the barrier energy between Li-ions, as it is shown in Equation (8)

$$D_s = D_0 e^{-\frac{E_a}{KT}} \tag{8}$$

It should be noticed that E_a is effective activation energy instead of actual activation energy to describe some energy barrier along diffusion pathways. In NMC materials, there is no observable structure displacement below 600 K. As in Equation (8), $\log(D_s)$ is linear to $1/T$, to compare the results from first-principle calculation with experimental results, linear fitting was applied to reach the diffusion coefficient at room temperature.

Also, cNEB method was performed to investigate the migration barrier of Li-ions in NMC layered materials.[28] cNEB was a complementary to NEB method. In this work, cNEB was applied in a $3 \times 3 \times 1$ supercell with five images as intermediate states. A series of images along the migration pathway were fully relaxed with a spring constant as constraint condition. Total energy of these series of intermediate states were calculated to describe the migration barrier along this pathway.

Supporting Information

Supporting Information is available from the Wiley Online Library or from the author.

Acknowledgements

S.C., Y.W. and T.L. contributed equally to this work. The work was financially supported by National Project for EV Batteries (20121110, OptimumNano, Shenzhen), the National Natural Science Foundation of China (No. 51302007), Guangdong Innovation Team Project (No. 2013N080), and Shenzhen Science and Technology Research Grant (Nos. ZDSY20130331145131323, CXZZ20120829172325895, JCYJ20130329181509637, and JCYJ20140417144423201). We also acknowledge the support of ShenZhen National Super Computing Center.

Received: July 1, 2015
Revised: October 19, 2015
Published online:

[1] M. Armand, J. M. Tarascon, *Nature* **2008**, *451*, 652.
[2] a) J. M. Tarascon, M. Armand, *Nature* **2001**, *414*, 359; b) H. Li, Z. Wang, L. Chen, X. Huang, *Adv. Mater.* **2009**, *21*, 4593.
[3] K. M. Shaju, G. V. Subba Rao, B. V. R. Chowdari, *J. Electrochem. Soc.* **2004**, *151*, A1324.
[4] a) X. Zhang, A. Mauger, W. J. Jiang, H. Groult, C. H. Julien, *ECS Transactions* **2011**, *35*, 89; b) K. C. Mahesh, H. Manjunatha, R. B. Shivashankaraiah, G. S. Suresh, T. V. Venkatesha, *J. Electrochem. Soc.* **2012**, *159*, A1040.
[5] a) J. K. Ngala, N. A. Chernova, M. Ma, M. Mamak, P. Y. Zavalij, M. S. Whittingham, *J. Mater. Chem.* **2004**, *14*, 214; b) M. Ma, N. A. Chernova, B. H. Toby, P. Y. Zavalij, M. S. Whittingham, *J. Power Sources* **2007**, *165*, 517.
[6] H. Yu, Y. Qian, M. Otani, D. Tang, S. Guo, Y. Zhu, H. Zhou, *Energy Environ. Sci.* **2014**, *7*, 1068.
[7] a) S. Yang, X. Wang, X. Yang, Y. Bai, Z. Liu, H. Shu, Q. Wei, *Electrochim. Acta* **2012**, *66*, 88; b) Z. Wu, X. Han, J. Zheng, Y. Wei, R. Qiao, F. Shen, J. Dai, L. Hu, K. Xu, Y. Lin, W. Yang, F. Pan, *Nano Lett.* **2014**, *14*, 4700; c) Z. Wu, S. Ji, J. Zheng, Z. Hu, S. Xiao, Y. Wei,

Z. Zhuo, Y. Lin, W. Yang, K. Xu, K. Amine, F. Pan, *Nano Lett.* **2015**, *15*, 5590.
[8] a) P. Y. Liao, J. G. Duh, S. R. Sheen, *J. Power Sources* **2005**, *143*, 212; b) P. Yue, Z. Wang, W. Peng, L. Li, H. Guo, X. Li, Q. Hu, Y. Zhang, *Scripta Mater.* **2011**, *65*, 1077; c) A. Yaqub, Y.-J. Lee, M. J. Hwang, S. A. Pervez, U. Farooq, J.-H. Choi, D. Kim, H.-Y. Choi, S.-B. Cho, C.-H. Doh, *J. Mater. Sci.* **2014**, *49*, 7707.
[9] a) L. Wang, J. G. Li, N. Chi, H. Y. Yu, T. Dong, *Adv. Mater. Res.* **2012**, *554*, 445; b) K. S. Lee, S. T. Myung, K. Amine, H. Yashiro, Y. K. Sun, *J. Electrochem. Soc.* **2007**, *154*, A971.
[10] H.-J. Noh, S. Youn, C. S. Yoon, Y.-K. Sun, *J. Power Sources* **2013**, *233*, 121.
[11] A. Van der Ven, G. Ceder, *Electrochem. Solid State Lett.* **2000**, *3*, 301.
[12] Y. Wei, J. Zheng, S. Cui, X. Song, Y. Su, W. Deng, Z. Wu, X. Wang, W. Wang, M. Rao, Y. Lin, C. Wang, K. Amine, F. Pan, *J. Am. Chem. Soc.* **2015**, *137*, 8364.
[13] W. Weppner, R. A. Huggins, *J. Electrochem. Soc.* **1977**, *124*, 1569.
[14] C. John Wen, B. A. Boukamp, R. A. Huggins, W. Weppner, *J. Electrochem. Soc.* **1979**, *126*, 2258.
[15] Y. J. Zhu, C. S. Wang, *J. Phys. Chem. C* **2010**, *114*, 2830.
[16] Z. Shen, L. Cao, C. D. Rahn, C. Y. Wang, *J. Electrochem. Soc.* **2013**, *160*, A1842.
[17] a) P. Yu, B. N. Popov, J. A. Ritter, R. E. White, *J. Electrochem. Soc.* **1999**, *146*, 8; b) M. D. Levi, G. Salitra, B. Markovsky, H. Teller, D. Aurbach, U. Heider, L. Heider, *J. Electrochem. Soc.* **1999**, *146*, 1279.
[18] a) C. Ho, I. D. Raistrick, R. A. Huggins, *J. Electrochem. Soc.* **1980**, *127*, 343; b) A. Funabiki, M. Inaba, Z. Ogumi, *J. Power Sources* **1997**, *68*, 227; c) K. Dokko, M. Mohamedi, Y. Fujita, T. Itoh, M. Nishizawa, M. Umeda, I. Uchida, *J. Electrochem. Soc.* **2001**, *148*, A422.
[19] a) R. S. Nicholson, *Anal. Chem.* **1965**, *37*, 1351; b) S.-I. Pyun, H.-C. Shin, *J. Power Sources* **2001**, *97–98*, 277.
[20] K. S. Kang, Y. S. Meng, J. Breger, C. P. Grey, G. Ceder, *Science* **2006**, *311*, 977.
[21] J. Xiao, N. A. Chernova, M. S. Whittingham, *Chem. Mater.* **2008**, *20*, 7454.
[22] a) Z. Li, C. Ban, N. A. Chernova, Z. Wu, S. Upreti, A. Dillon, M. S. Whittingham, *J. Power Sources* **2014**, *268*, 106; b) M. Park, X. Zhang, M. Chung, G. B. Less, A. M. Sastry, *J. Power Sources* **2010**, *195*, 7904.
[23] a) G. Kresse, J. Hafner, *Phys. Rev. B* **1993**, *47*, 558; b) G. Kresse, J. Hafner, *Phys. Rev. B* **1994**, *49*, 14251; c) G. Kresse, J. Furthmüller, *Phys. Rev. B* **1996**, *54*, 11169.
[24] J. P. Perdew, K. Burke, M. Ernzerhof, *Phys. Rev. Lett.* **1996**, *77*, 3865.
[25] Z. Wu, R. E. Cohen, *Phys. Rev. B* **2006**, *73*, 235116.
[26] B. Hwang, Y. Tsai, D. Carlier, G. Ceder, *Chem. Mater.* **2003**, *15*, 3676.
[27] a) I. M. Markus, F. Lin, K. C. Kam, M. Asta, M. M. Doeff, *J. Phys. Chem. Lett.* **2014**, *5*, 3649; b) H. Yu, Y. Qian, M. Otani, D. Tang, S. Guo, Y. Zhu, H. Zhou, *Energy Environ. Sci.* **2014**, *7*, 1068.
[28] a) G. Henkelman, H. Jónsson, *J. Chem. Phys.* **2000**, *113*, 9978; b) G. Henkelman, B. P. Uberuaga, H. Jónsson, *J. Chem. Phys.* **2000**, *113*, 9901.
[29] a) A. Van der Ven, G. Ceder, *Electrochem. Commun.* **2004**, *6*, 1045; b) J. Breger, K. Kang, J. Cabana,G. Ceder, C. P. Grey, *J. Mater. Chem.* **2007**, *17*, 3167.
[30] M. M. Thackeray, S.-H. Kang, C. S. Johnson, J. T. Vaughey, R. Benedek, S. A. Hackney, *J. Mater. Chem.* **2007**, *17*, 3112.